JOURNAL OF MAGNETIC RESONANCE 98, 443–450 (1992)

4D NMR Triple-Resonance Experiments for Assignment of Protein Backbone Nuclei Using Shared Constant-Time Evolution Periods

LEWIS E. KAY,* MICHAEL WITTEKIND,† MARK A. MCCOY,†
MARK S. FRIEDRICHS,† AND LUCIANO MUELLER†,‡

** Departments of Medical Genetics, Biochemistry, and Chemistry, University of Toronto, Toronto, Canada; and † Macromolecular NMR Department, Bristol-Myers Squibb Pharmaceutical Research Institute, Princeton, New Jersey 08543*

Received March 10, 1992

Recently triple-resonance multidimensional NMR experiments have been developed which enable the assignment of backbone atoms in ^{15}N,^{13}C-labeled proteins, based exclusively on scalar connectivities (*1, 2*). These experiments offer a very powerful alternative to the more conventional approach which relies on sequential assignments of proteins via through-space connectivities. The power of the triple-resonance approach has been demonstrated with a number of different proteins (*2–6*).

In this Communication we introduce two new 4D NMR triple-resonance experiments, the HNCAHA and the HN(CO)CAHA experiments. As will be described later, these two experiments in concert offer a powerful approach to the assignment of backbone atoms in ^{15}N,^{13}C-labeled proteins. The HNCAHA experiment correlates the intraresidue ^1HN, ^{15}N, $^{13}C_\alpha$, and $^1H_\alpha$ chemical shifts by transferring magnetization originating on the ^1HN proton to $^1H_\alpha$ via the pathway

$$^1HN^{(i)} \xrightarrow{J_{NH}} {}^{15}N^{(i)} \xrightarrow{J_{NC\alpha}} {}^{13}C_\alpha^{(i)} \xrightarrow{J_{C\alpha H\alpha}} {}^1H_\alpha^{(i)},$$

where J_{NH}, $J_{NC\alpha}$, and $J_{C\alpha H\alpha}$ are the one-bond ^{15}N–^1HN, ^{15}N–$^{13}C_\alpha$, and $^{13}C_\alpha$–$^1H_\alpha$ coupling constants, respectively. Magnetization is returned to the ^1HN spins for detection during t_4, with the chemical shifts of the $^{13}C_\alpha$, $^1H_\alpha$, and ^{15}N nuclei recorded during t_1, t_2, and t_3, respectively. If the ratio of the two-bond coupling ($J_{NC\alpha'}$) between the ^{15}N spin of residue i and the $^{13}C_\alpha$ spin of the preceding residue $i-1$ and the ^{15}N transverse relaxation time is sufficiently large, a cross peak is observed connecting the ^1HN and ^{15}N spins of a given residue with the $^1H_\alpha$ and $^{13}C_\alpha$ spins of the preceding residue.

The HN(CO)CAHA experiment correlates the ^1HN and ^{15}N shifts of residue i with the $^1H_\alpha$ and $^{13}C_\alpha$ shifts of residue $i-1$ by transferring magnetization through the intervening carbonyl spin (C). The pathway of magnetization transfer can be indicated schematically as

$$^1HN^{(i)} \xrightarrow{J_{NH}} {}^{15}N^{(i)} \xrightarrow{J_{NC}} {}^{13}C^{(i-1)} \xrightarrow{J_{CC\alpha}} {}^{13}C_\alpha^{(i-1)} \xrightarrow{J_{C\alpha H\alpha}} {}^1H_\alpha^{(i-1)},$$

‡ To whom correspondence should be addressed.

0022-2364/92 $5.00

where J_{NC} and $J_{CC\alpha}$ are the one-bond ^{15}N–^{13}C and ^{13}C–$^{13}C^{\alpha}$ coupling constants, respectively. As in the HNCAHA experiment, magnetization is returned to the ^{1}HN spin for detection during t_4 with the chemical shifts of the $^{13}C_{\alpha}$, $^{1}H_{\alpha}$, and ^{15}N nuclei recorded during t_1, t_2, and t_3, respectively. Very recently, Boucher *et al.* developed a pair of related experiments where $^{1}H_{\alpha}$ magnetization first evolves in t_1 and is subsequently relayed to the C_{α} carbon and the amide nitrogen, where it evolves during the t_2 and t_3 period, respectively (*12*). As in our method, amide proton magnetization is detected during the t_4 period.

The HNCAHA and the HN(CO)CAHA experiments are extensions of the previously published 3D HNCA (*1*) and HN(CO)CA (*7*) pulse sequences. A particularly novel feature of the 4D experiments presented here, however, is that two of the four chemical shifts are recorded simultaneously, providing an increase in the sensitivity of the resultant spectra which is discussed in more detail below. Furthermore, recording of the ^{15}N evolution can also be accomplished using the constant-time approach by shifting the position of the 180° pulse pair in the back-transfer period between intervals t_N^1 and t_N^2. Hence, the proposed sequences represent truly constant-time four-dimensional experiments where the interval between the first excitation pulse and the detection period remains constant throughout the entire four-dimensional data collection.

Figure 1 shows the pulse sequences that were used to record the HNCAHA (Fig. 1A) and the HN(CO)CAHA (Fig. 1B) experiments. The coherence pathways in these experiments are most readily described in terms of the product-operator formalism (*8*). We present a product-operator description of the HNCAHA experiment. In this description, the effects of relaxation are neglected, only those terms which contribute to observed magnetization are retained, numerical factors preceding the operators are omitted for simplicity, and the interresidue transfer of magnetization via the two-bond ^{15}N–$^{13}C_{\alpha}$ coupling, $J_{NC\alpha'}$, is neglected. In addition, the first phase of all the pulses indicated in the legend to Fig. 1 is employed. The following operator symbols are used: I for the ^{1}HN spin, N for the ^{15}N spin, C_{α} for the intraresidue $^{13}C_{\alpha}$ spin, H for the intraresidue $^{1}H_{\alpha}$ spin, C'_{α} for the interresidue $^{13}C_{\alpha}$ spin, H′ for the interresidue $^{1}H_{\alpha}$ spin, and C for the carbonyl spin.

At time *a* the magnetization, ρ, is given by $\rho_a = I_z$. Magnetization is transferred via an INEPT (*9*) transfer to ^{15}N, giving at time *b*

$$\rho b = I_z N_y \sin(2\pi J_{NH}\tau'). \quad [1]$$

The antiphase ^{15}N magnetization is allowed to refocus with respect to the coupled HN proton during 2τ and dephasing due to the ^{15}N–$^{13}C_{\alpha}$ coupling occurs during the delay $2\delta_1$, yielding at time *c*

$$\rho c = N_y C_{\alpha z} \sin(2\pi J_{NC\alpha}\delta_1)\cos(2\pi J_{NC\alpha'}\delta_1). \quad [2]$$

In the derivation of Eq. [2] we have assumed that 2τ is set to exactly $1/(2J_{NH})$. ^{1}H decoupling is applied immediately following the 2τ period to ensure that ^{15}N magnetization remains in phase with respect to the coupled ^{1}HN spin. (In what follows, trigonometric terms from preceding expressions will not be carried over and will be included only in the expression for the detected magnetization.) Note that carbonyl decoupling is applied in the sequence whenever transverse ^{15}N magnetization is present and therefore ^{15}N magnetization does not evolve due to the ^{15}N–^{13}C coupling.

Simultaneous application of ^{15}N and $^{13}C_{\alpha}$ pulses yields at time *d*

$$\rho d = N_z C_{\alpha y}. \quad [3]$$

$^{13}C_\alpha$ magnetization is allowed to evolve under ^1H coupling during δ_2, yielding at time e a term of the form

$$\rho e = N_z C_{\alpha x} H_z \sin(\pi J_{C\alpha H\alpha} \delta_2). \quad [4]$$

The evolution of spin C_α due to chemical shift and due to ^{15}N–$^{13}C_\alpha$ scalar coupling during δ_2 is neglected since refocusing occurs later in the sequence. Note that between the $90^\circ_{\phi 3}$ $^{13}C_\alpha$ pulse and the next 90° $^{13}C_\alpha$ pulse carbon magnetization evolves for a time $2T + 2\delta_2$ due to the one-bond $^{13}C_\alpha$–$^{13}C_\beta$ coupling, $J_{C\alpha C\beta}$. This introduces an attenuation factor of the form $\cos\{2\pi J_{C\alpha C\beta}(T + \delta_2)\}$ in the expression for the final magnetization (see Eqs. [8] and [9]). Application of a ^1H 90° pulse yields

$$\rho f = N_z C_{\alpha x} H_y. \quad [5]$$

Both $^1H_\alpha$ and $^{13}C_\alpha$ chemical shifts are recorded simultaneously during the constant-time period, $2T$. This can be accomplished, as we have done, by enabling the ^1H and $^{13}C_\alpha$ 180° pulses ($180^\circ_{\phi 5}$ and $180^\circ_{\phi 6}$) to cross each other during the course of the t_1, t_2 evolution periods. Alternatively, these two echo pulses can be moved in opposite directions, for example by letting the ^1H 180° pulse move to the right in t_2, thus avoiding any overlap of these pulses except for $t_1 = t_2 = 0$. It is important to note that the evolution of $C_{\alpha x}H_y$ (double- and zero-quantum ^1H–$^{13}C_\alpha$ magnetization) proceeds during $2T$ in a manner independent of the $^1H_\alpha$–$^{13}C_\alpha$ coupling for all common amino acid residues except for glycine (*8*). This permits the recording of the $^{13}C_\alpha$ and $^1H_\alpha$ chemical shifts without the effects of the large one-bond scalar coupling during simultaneous constant-time periods.

At time g, ρg is given by

$$\rho g = N_z C_{\alpha y} \sin(\pi J_{C\alpha H\alpha} \delta_2) \cos(\omega_{C\alpha} t_1) \cos(\omega_{H\alpha} t_2), \quad [6]$$

where the effects of scalar coupling between the $^{13}C_\alpha$ and ^{15}N spins during t_1 and the coupling between ^1HN and $^1H_\alpha$ spins during t_2 are neglected. In Eq. [6], $\omega_{C\alpha}$ and $\omega_{H\alpha}$ are the $^{13}C_\alpha$ and $^1H_\alpha$ angular frequencies, respectively. Magnetization is transferred back to the ^1HN spins by the reverse of the path described above so that at time h the magnetization is given by

$$\rho h = N_y I_z \sin(2\pi J_{NC\alpha} \delta_1) \cos(2\pi J_{NC\alpha'} \delta_1) \cos(\omega_N t_3), \quad [7]$$

where ω_N is the ^{15}N angular frequency. The ^{15}N–$^{13}C_\alpha$ scalar coupling is neglected during t_3 in the derivation of Eq. [7]. The ^1H decoupling that occurs via the MLEV (*10*) sequence during t_3 ensures that ^{15}N evolution does not occur due to J_{NH}. Finally, the last INEPT transfer returns magnetization to the ^1HN spin and at a time i the magnetization is given by

$$\rho i = I_x \sin^2(2\pi J_{NH}\tau') \sin^2(\pi J_{C\alpha H\alpha} \delta_2) \sin^2(2\pi J_{NC\alpha} \delta_1) \cos^2(2\pi J_{NC\alpha'} \delta_1)$$
$$\times \cos\{2\pi J_{C\alpha C\beta}(T + \delta_2)\} \cos(\omega_{C\alpha} t_1) \cos(\omega_{H\alpha} t_2) \cos(\omega_N t_3), \quad [8]$$

where all the relevant trigonometric terms are now included. For those cases where a sequential cross peak is also observed, ρi is given by

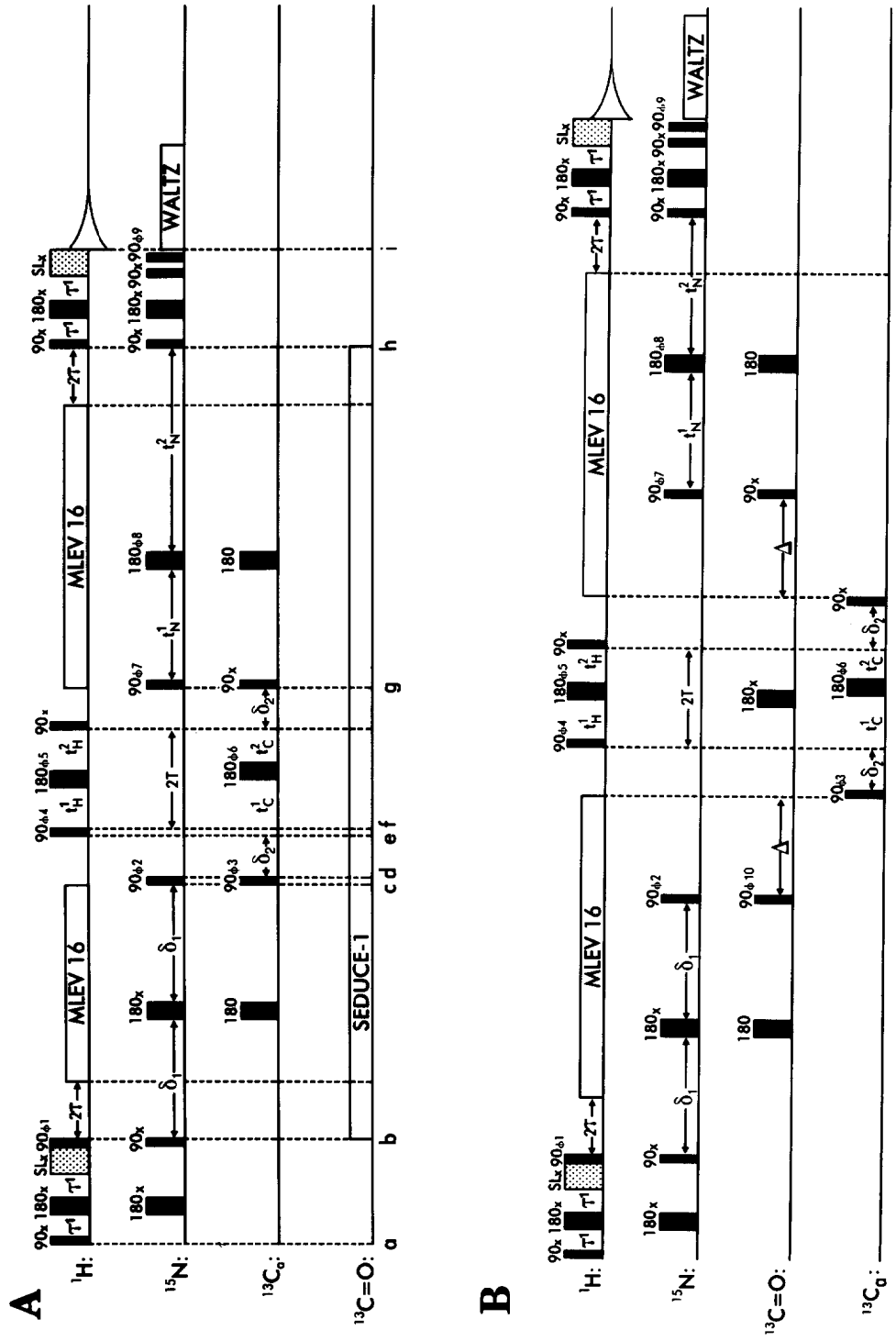
A
B
MLEV 16
SEDUCE-1
WALTZ
2T
Δ
a
b
c d e f
g
h
i

$$\rho i = I_x \sin^2(2\pi J_{NH}\tau')\sin^2(\pi J_{C\alpha H\alpha}\delta_2)\cos(\omega_N t_3)\cos\{2\pi J_{C\alpha C\beta}(T+\delta_2)\}$$
$$\times [\sin^2(2\pi J_{NC\alpha}\delta_1)\cos^2(2\pi J_{NC\alpha'}\delta_1)\cos(\omega_{C\alpha}t_1)\cos(\omega_{H\alpha}t_2)$$
$$+ \sin^2(2\pi J_{NC\alpha'}\delta_1)\cos^2(2\pi J_{NC\alpha}\delta_1)\cos(\omega_{C\alpha'}t_1)\cos(\omega_{H\alpha'}t_2)], \quad [9]$$

where $\omega_{C\alpha'}$ and $\omega_{H\alpha'}$ are the carbon and proton angular frequencies associated with the sequential peak.

The values of δ_1, δ_2, and T are optimized for maximum sensitivity in a manner described previously (*11*). For values of ($J_{NC\alpha}$, $J_{NC\alpha'}$, $J_{C\alpha C\beta}$, $J_{C\alpha H\alpha}$, $T_2[^{15}N]$, $T_2[^{13}C_\alpha]$) = 11 Hz, 7 Hz, 35 Hz, 140 Hz, 50 ms, 16 ms) optimum values of (δ_1, δ_2, T) are (12, 2.6, 1.5 ms). The value of τ' is set to slightly less than $1/(4J_{NH})$.

The description of the relevant magnetization-transfer steps in the HN(CO)CAHA experiment is very similar to that of the HNCAHA sequence outlined above and therefore only the differences in the two sequences will be described here. In the HNCAHA experiment, during the δ_1 periods, ^{15}N magnetization is allowed to evolve due to the ^{15}N–$^{13}C_\alpha$ scalar coupling while the effects of the carbonyl–^{15}N scalar coupling, J_{NC}, are suppressed by carbonyl decoupling. In contrast, during the δ_1 periods in the HN(CO)CAHA experiment, ^{15}N magnetization evolves due to J_{NC}, while evolution due to the ^{15}N–$^{13}C^\alpha$ coupling is refocused by the application of the ^{15}N 180° pulse in the center of the δ_1 evolution periods. Note that, in the HN(CO)CAHA pulse scheme, it is necessary that carbonyl pulses have minimal excitation in the $^{13}C_\alpha$ region of the carbon spectrum and vice versa. A second difference between the sequences is that the HN(CO)CAHA scheme includes a period, Δ, during which carbonyl magnetization evolves due to the one-bond carbonyl–$^{13}C_\alpha$ coupling, $J_{CC\alpha}$. During the first Δ period, carbonyl magnetization dephases due to $J_{CC\alpha}$ and subsequent application of the $^{13}C_\alpha$ $90^\circ_{\phi 3}$ pulse creates double- and zero-quantum carbonyl–$^{13}C_\alpha$ magnetization. Simultaneous recording of the $^{13}C_\alpha$ and $^1H_\alpha$ chemical shifts occurs during $2T$, while the carbonyl chemical shift is refocused by the carbonyl 180° pulse applied in the

---

FIG. 1. Pulse schemes for the HNCAHA (A) and HN(CO)CAHA (B) experiments. Water suppression is achieved for both sequences using presaturation. The suppression of water is aided by the application of spin-lock pulses (*13*). The first spin-lock pulse is set to 2 ms in the HNCAHA experiment and 1 ms in the HN(CO)CAHA experiment. The second spin-lock pulse was not used in either experiment. In each experiment, quadrature detection in t_1, t_2, and t_3 was obtained using the States–TPPI method (*14*), with ϕ_3, ϕ_4, and ϕ_7 incremented independently. The value of τ' is set to 2.5 ms [slightly less than $1/(4J_{NH})$] while the value of τ is set to 2.7 ms [$=1/(4J_{NH})$]. The values of δ_2 and T are set to 2.6 and 1.5 ms, respectively; $t_C^1 = T + (t_1/2)$, $t_C^2 = T - (t_1/2)$, $t_H^1 = T + (t_2/2)$, $t_H^2 = T - (t_2/2)$, $t_N^1 = \delta_1$, $t_N^2 = \delta_1 + t_3$. For the F_3 constant-time variation, $t_N^1 = \delta_1 + (t_3/2)$, $t_N^2 = \delta_1 - (t_3/2)$. In the HNCAHA experiment all carbon pulses are as short as possible (~13 μs for a carbon 90° pulse). Carbonyl decoupling is achieved in the HNCAHA experiment using the shaped decoupling sequence SEDUCE-1 (*15*). The phase-cycling scheme used for the HNCAHA sequence is as follows: $\phi_1 = y, -y$; $\phi_2 = 2(x), 2(-x)$; $\phi_3 = x$; $\phi_4 = x$; $\phi_5 = 4(x), 4(y)$; $\phi_6 = 8(x), 8(y), 8(-x), 8(-y)$; $\phi_7 = x$; $\phi_8 = x$; $\phi_9 = 16(x), 16(-x)$; Rec = $x, 2(-x), x, -x, 2(x), -x, -x, 2(x), -x, x, 2(-x), x$. The value of δ_1 is set to 12 ms. In the HN(CO)CAHA experiment, the radiofrequency field strength of the carbonyl and $^{13}C_\alpha$ RF channels is adjusted such that a 90° $^{13}C_\alpha$ pulse causes minimal excitation in the carbonyl region and vice versa. This requires that a 90° pulse length of ~53 μs be employed for a carbon frequency of 150.9 MHz. The phase-cycling scheme used for the HN(CO)CAHA sequence is as follows: $\phi_1 = y, -y$; $\phi_2 = 2(x), 2(-x)$; $\phi_3 = x$; $\phi_4 = x$; $\phi_5 = 4(x), 4(y)$; $\phi_6 = 8(x), 8(y), 8(-x), 8(-y)$; $\phi_7 = x$; $\phi_8 = x$; $\phi_9 = 16(x), 16(-x)$; $\phi_{10} = 16(x), 16(-x)$; Rec = $x, 2(-x), x, -x, 2(x), -x, 2[-x, 2(x), -x, x, 2(-x), x], x, 2(-x), x, -x, 2(x), -x$. The value of δ_1 is set to 12.5 ms.

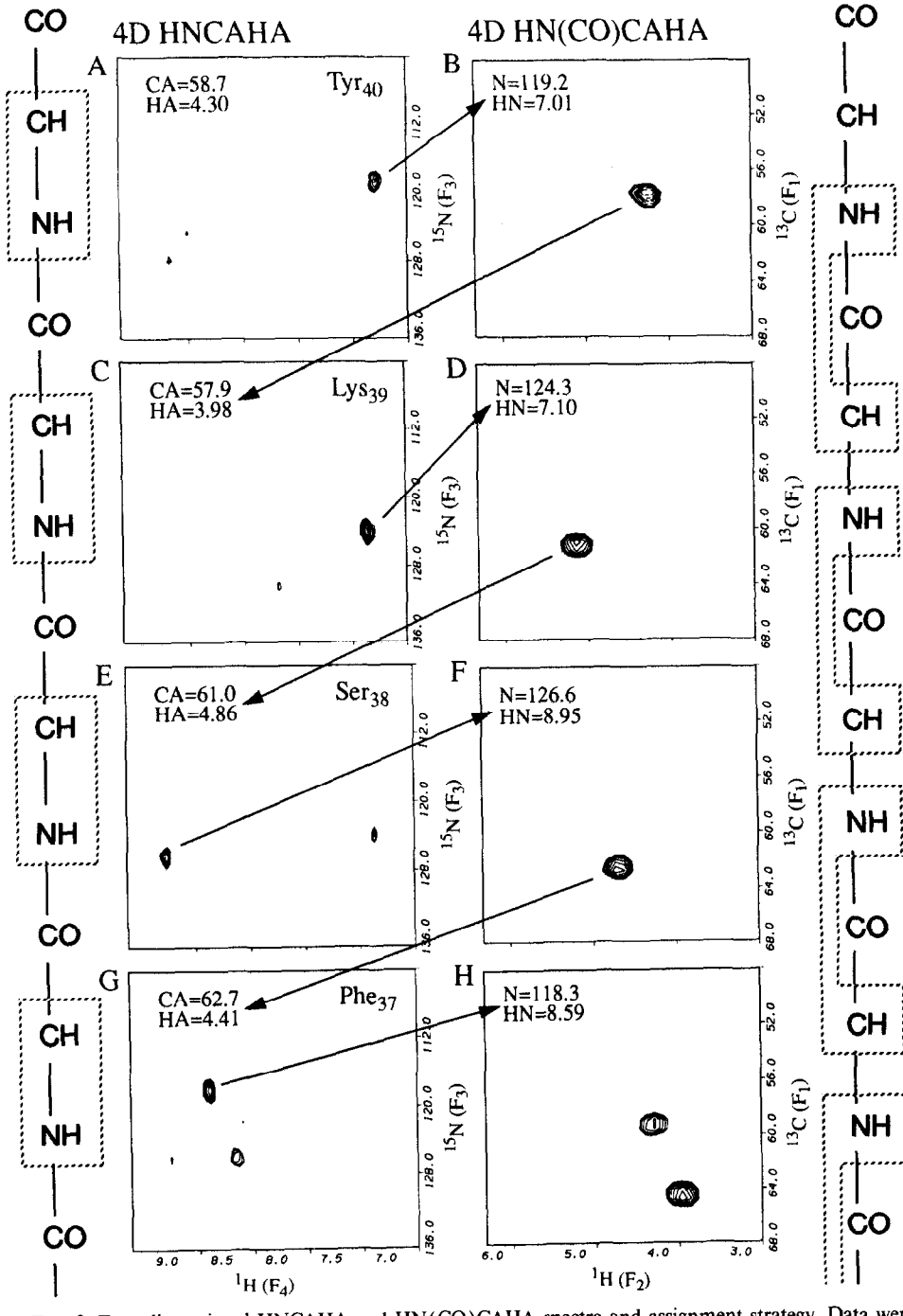

FIG. 2. Four-dimensional HNCAHA and HN(CO)CAHA spectra and assignment strategy. Data were collected using the pulse sequences outlined in the legend to Fig. 1 without the F_3 constant-time variation. Two-dimensional slices of the 4D spectra recorded for the 93-residue RNA-binding domain of hnRNP C are shown in the different panels. F_3, F_4 slices of the 4D HNCAHA spectrum (A, C, E, G) and F_1, F_2 slices of the 4D HN(CO)CAHA spectrum (B, D, F, H) are shown. The fixed frequencies are displayed in the top

center of the constant-time period $2T$ (Fig. 1B). We note that the dimensionality of this experiment could easily be extended to five simply by moving the carbonyl 180° pulse during the constant-time period $2T$, allowing for the detection of the carbonyl frequencies in the additional dimension.

Immediately before acquisition the magnetization is given by

$$\rho = I_x \sin^2(2\pi J_{NH}\tau')\sin^2(2\pi J_{NC}\delta_1)\sin^2(\pi J_{CC\alpha}\Delta)\sin^2(\pi J_{C\alpha H\alpha}\delta_2) \times \cos\{2\pi J_{C\alpha C\beta}(T + \delta_2)\}\cos(\omega_{C\alpha'}t_1)\cos(\omega_{H\alpha'}t_2)\cos(\omega_N t_3). \quad [10]$$

In the derivation of Eq. [10], the scalar coupling between the ^{15}N and $^{13}C_\alpha$ spins during t_1 and the coupling between the ^1HN and $^1H_\alpha$ nuclei during t_2 have been neglected. The delays δ_1, Δ, δ_2, and T in Eq. [10] are readily optimized for maximum sensitivity (*11*). For values of (J_{NC}, $J_{CC\alpha}$, $J_{C\alpha C\beta}$, $J_{C\alpha H\alpha}$, $T_2[^{13}C]$, $T_2[^{13}C_\alpha]$) = 15 Hz, 55 Hz, 35 Hz, 140 Hz, 50 ms, 16 ms) optimal delays (δ_1, Δ, δ_2, T = 12.5, 4.2, 2.6, 1.5 ms) are chosen. As in the HNCAHA experiment, the value of τ' is set slightly less than $1/(4J_{NH})$.

The 4D HNCAHA and HN(CO)CAHA experiments are demonstrated on a 93-amino-acid protein fragment corresponding to the RNA-binding domain (RBD) of the hnRNP C protein. The ^1H, ^{15}N, and ^{13}C resonance assignments for the hnRNP C RBD have been previously determined (*6*). The protein concentration was 3 m*M* in 50 m*M* sodium acetate, 100 μ*M* EDTA, pH 5.5, in 91% ^1H_2O/9% ^2H_2O. Data were collected at 20°C on a Varian UNITY 600 spectrometer equipped with a triple-resonance probe.

The approach used to identify and visualize sequential connectivities between amino acid residues is illustrated in Fig. 2 for residues Phe_{37} through Tyr_{40} of the hnRNP C RBD sequence. The Tyr_{40} intraresidue cross peak in the HNCAHA spectrum is viewed by fixing at the $F_1[^{13}C_\alpha]$ and $F_2[^1H_\alpha]$ dimensions, resulting in a 2D plot with the $F_3[^{15}N]$ and $F_4[^1HN]$ axis displayed (Fig. 2A). The ^{15}N and ^1HN frequencies of Tyr_{40} determined in this plot are used as the fixed frequencies for the F_3 and F_4 dimensions of the HN(CO)CAHA spectrum, resulting in an F_1–F_2 2D plot (Fig. 2B) in which an interresidue cross peak at the $^{13}C_\alpha$ and $^1H_\alpha$ frequencies of Lys_{39} is displayed. These Lys_{39} $^{13}C_\alpha$ and $^1H_\alpha$ frequencies are then used to fix the frequencies of the F_1 and F_2 dimensions of the HNCAHA spectrum, resulting in the visualization of the Lys_{39} intraresidue cross peak in the F_3–F_4 2D plot shown in Fig. 2C. The next linkage is established by using the newly determined Lys_{39} ^{15}N and ^1HN resonances as the fixed F_3 and F_4 frequencies for the HN(CO)CAHA spectrum, resulting in the display of the interresidue Lys_{39}–Ser_{38} cross peak (Fig. 2D). Note that weak interresidue cross peaks correlating $F_1[^{13}C_\alpha(i-1)]$, $F_2[^1H_\alpha(i-1)]$, $F_3[^{15}N]$, $F_4[^1HN(i)]$ are visible in some of the HNCAHA panels (Figs. 2E and 2G).

---

left corner of each panel. The arrows indicate how the resonance positions of the cross peaks are used to derive the frequencies of the fixed dimensions for the subsequent panels (see text for details). Schematic representations of the protein backbone atoms are depicted next to the two sets of panels. The dotted boxes indicate the relevant atom correlations that give rise to the cross peaks shown in the adjacent panels. The spectra were recorded with spectral widths of 3000, 3125, 2000, and 6250 Hz with acquisition times of 2.56, 2.67, 8.0, and 41.8 ms in the $F_1[^{13}C_\alpha]$, $F_2[^1H_\alpha]$, $F_3[^{15}N]$, and $F_4[^1HN]$ dimensions, respectively. The data were transformed into 32 × 32 × 64 × 128-real-point matrices. Mirror-image linear prediction (*16*) was used to extend the data from 8 to 24 points in the F_1 and F_2 dimensions prior to cosine bell apodization, zero-filling to 32 points, and Fourier transformation. Data processing was performed using a modified version of the program FELIX (Hare Research, Bothel, Washington; M. S. Friedrichs, unpublished).

This process of linking intraresidue HNCAHA peaks via interresidue HN(CO)CAHA peaks is continued until an ambiguity is reached. For example, a potential ambiguity arises in Fig. 2H, as two peaks are visible in this view. However, the true Phe_{37}–Ile_{36} sequential peak at F_1 = 64.3 ppm, F_2 = 3.72 ppm is centered on the fixed F_3–F_4 dimensions while the other peak at F_1 = 59.8 ppm, F_2 = 4.05 ppm is centered on an adjacent slice, so the assignment process can be continued.

Recently Boucher *et al.* have developed a similar approach for the assignment of backbone resonances in labeled proteins based on recording two 4D experiments (*12*). One of these experiments, called the HCA(CO)NNH experiment, links the $^1H_\alpha$ and $^{13}C_\alpha$ shifts of residue $i-1$ with the ^{15}N and ^1HN shifts of residue i. The other experiment, HCANNH, links intraresidue $^1H_\alpha$, $^{13}C_\alpha$, ^{15}N, and ^1HN chemical shifts by transferring net magnetization from the $^1H_\alpha$ spin to the ^1HN spin. The set of experiments developed by Boucher *et al.* and the experiments proposed here should be equally applicable for the backbone assignment of small proteins (<15 kDa). However, it is anticipated that for studies of larger proteins the HCANNH experiment will suffer most seriously from losses in sensitivity due to the short $^{13}C_\alpha$ T_2 values in large proteins.

In summary, we have presented two new 4D triple-resonance NMR experiments for obtaining backbone assignments of ^{15}N,^{13}C-labeled proteins. The experiments incorporate a novel double constant-time period which enables simultaneous recording of the $^{13}C_\alpha$ and $^1H_\alpha$ chemical shifts. This approach can be easily extended in the HN(CO)CAHA experiment to encode the carbonyl frequencies during the same constant-time period, resulting in a five-dimensional experiment. Because spectra are recorded with a single sample and under a single set of conditions, it should be possible to automate the assignment procedure in a very straightforward fashion.

ACKNOWLEDGMENT

We thank Louise Zingale for assistance with the preparation of the manuscript.

REFERENCES

1. L. E. KAY, M. IKURA, R. TSCHUDIN, AND A. BAX, *J. Magn. Reson.* **89,** 496 (1990).
2. M. IKURA, L. E. KAY, AND A. BAX, *Biochemistry* **29,** 4659 (1990).
3. M. IKURA, L. E. KAY, M. KRINKS, AND A. BAX, *Biochemistry* **30,** 5498 (1991).
4. J. G. PELTON, D. A. TORCHIA, N. D. MEADOW, C. Y. WONG, AND S. ROSEMAN, *Biochemistry* **30,** 10,043 (1991).
5. R. POWERS, G. M. CLORE, A. BAX, D. GARRETT, S. STAHL, P. T. WINGFIELD, AND A. M. GRONENBORN, *J. Mol. Biol.* **221,** 108 (1991).
6. M. WITTEKIND, M. GORLACH, M. S. FRIEDRICHS, G. DREYFUSS, AND L. MUELLER, *Biochemistry,* submitted.
7. A. BAX AND M. IKURA, *J. Biomol. NMR.* **1,** 99 (1991).
8. R. R. ERNST, G. BODENHAUSEN, AND A. WOKAUN, "Principles of Nuclear Magnetic Resonance in One and Two Dimensions," pp. 25–32, Clarendon Press, Oxford, 1987.
9. G. A. MORRIS AND R. FREEMAN, *J. Am. Chem. Soc.* **99,** 760 (1979).
10. M. H. LEVITT AND R. FREEMAN, *J. Magn. Reson.* **43,** 502 (1981).
11. L. E. KAY, M. IKURA, AND A. BAX, *J. Magn. Reson.* **91,** 84 (1991).
12. W. BOUCHER, E. D. LAUE, P. J. DOMAILLE, AND S. CAMPBELL-BURK, *J. Am. Chem. Soc.* **114,** 2262 (1992).
13. B. A. MESSERLE, G. WIDER, G. OTTING, C. WEBER, AND K. WÜTHRICH, *J. Magn. Reson.* **85,** 658 (1989).
14. D. MARION, M. IKURA, R. TSCHUDIN, AND A. BAX, *J. Magn. Reson.* **85,** 393 (1989).
15. M. A. MCCOY AND L. MUELLER, *J. Am. Chem. Soc.* **114,** 2108 (1992).
16. G. ZHU AND A. BAX, *J. Magn. Reson.* **90,** 405 (1990).